Supporting Information for

"Goos-Hänchen Shift and Even-Odd Peak Oscillations in Edge-Reflections of Surface Polaritons in Atomically Thin Crystals"

Ji-Hun Kang[1†], Sheng Wang[1,2†], Zhiwen Shi[3,4*], Wenyu Zhao[1,5], Eli Yablonovitch[2,6,7], and Feng Wang[1,2,7*]

[1] Department of Physics, University of California at Berkeley, Berkeley, California 94720, USA

[2] Materials Science Division, Lawrence Berkeley National Laboratory, Berkeley, California 94720, USA

[3] Key Laboratory of Artificial Structures and Quantum Control (Ministry of Education), Department of Physics and Astronomy, Shanghai Jiao Tong University, Shanghai 200240, China

[4] Collaborative Innovation Center of Advanced Microstructures, Nanjing 210093, China

[5] Department of Physics, Harbin Institute of Technology, Harbin 150001, China

[6] Department of Electrical Engineering and Computer Science, University of California at Berkeley, Berkeley, California 94720, USA

[7] Kavli Energy NanoSciences Institute at the University of California, Berkeley and the Lawrence Berkeley National Laboratory, Berkeley, California 94720, USA

[†]These authors contributed equally to this work

[*]fengwang76@berkeley.edu; zwshi@sjtu.edu.cn

1. Analytic theory on the edge-reflection of two-dimensional surface polaritons

1-1 Coupled mode theory

In order to describe the edge reflection of two-dimensional surface polaritons (2DSPs), we assume that there is a semi-infinite thin metal film of negative permittivity ε_m, surrounded by a medium having positive permittivity $\varepsilon_s << |\varepsilon_m|$, as shown in Fig. S1(a). To simplify the problem, we assume that every permittivity is real so that the whole system is lossless. For the excitation of surface polaritons, we consider the transverse-magnetic field configuration (E_x, E_y, and H_z). It can be shown that the 2DSP propagating along x-direction is governed by the following eigenvalue equation[1]

$$e^{ih\sqrt{\varepsilon_m k_0^2 - q_x^2}}\left(\varepsilon_m\sqrt{\varepsilon_s k_0^2 - q_x^2} - \varepsilon_s\sqrt{\varepsilon_m k_0^2 - q_x^2}\right) - \left(\varepsilon_m\sqrt{\varepsilon_s k_0^2 - q_x^2} + \varepsilon_s\sqrt{\varepsilon_m k_0^2 - q_x^2}\right) = 0 \qquad (1.1).$$

Here, $h \ll \lambda_0$ is the thickness of the thin metal. The solution of Eq. (1.1) can be approximately found as $q_x \approx -2\varepsilon_s / (h\varepsilon_m)$. The z-component magnetic field H_z with this eigenvalue has an anti-symmetric configuration such that its phase is anti-symmetric along y-direction[1].

When propagating 2DSPs meet the edge of the metal at x=0, one can naturally expect that 2DSPs get reflected because there is discontinuity in surface conductivity at the edge. However, we note that the origin of the reflection is actually the diffraction of 2DSPs. We can invoke Huygens-Fresnel principle[2] to describe a macroscopic procedure of the edge-reflection in the following three steps. First, 2DSPs that have arrived at the edge generate dipole light sources along the boundary (x=0, y), as shown in Fig. S1(b). After that, those dipole sources generate electromagnetic waves to both forward (directing to x<0) and backward (directing to x>0) directions. At last, as described in Fig. S3(c), the forward-directing waves couple out to the free-space, whereas the backward ones

couple to both 2DSPs and unbounded diffracting waves. Here, we note that the diffracting waves in free-space (x<0) and thin metal (x>0) regions can be completely described in terms of linearly independent basis functions of respective regions. In the free-space region (x<0), the basis function is obviously a plane-wave so that the forward diffracting waves can be expanded in the plane-wave bases. For infinitesimally thin metal, one can find that the basis function for the unbounded waves is $B\left(y,k_y\right)\equiv\left(y/|y|\right)\left[e^{ik_y|y|}+\left(k_y-q_y\right)\left(k_y+q_y\right)^{-1}e^{-ik_y|y|}\right]$ which satisfies the orthogonal condition such that

$$\int_{-\infty}^{\infty}dyB\left(y,k_y\right)B^*\left(y,k_{y1}\right)=4\pi\delta\left(k_y-k_{y1}\right)+\frac{k_{y1}+q_y}{k_{y1}-q_y}4\pi\delta\left(k_y+k_{y1}\right),$$
$$\int_{-\infty}^{\infty}dy\frac{y}{|y|}e^{iq_yy}B^*\left(y,k_y\right)=0,$$

where $q_y\equiv\sqrt{\varepsilon_sk_0^2-q_x^2}$. Given basis functions, we can write the complete description of H_z field distribution of the system as the followings:

$$\begin{aligned}H_z^{x\geq0}\left(x,y\right)&=\frac{y}{|y|}\left(e^{-iq_xx}-Re^{iq_xx}\right)e^{iq_y|y|}+\int_{-\infty}^{\infty}dk_y\rho\left(k_y\right)B\left(y,k_y\right)e^{ik_xx},\\H_z^{x\leq0}\left(x,y\right)&=\int_{-\infty}^{\infty}dk_y\tau\left(k_y\right)e^{ik_yy-ik_xx}\end{aligned}\qquad(1.2).$$

Here, $k_x\equiv\sqrt{\varepsilon_sk_0^2-k_y^2}$, R is the reflection coefficient of 2DSP, and $\rho\left(k_y\right)$ and $\tau\left(k_y\right)$ respectively are amplitudes of backward- and forward-diffracting wave components. We assumed that the metal film is infinitesimally thin so that we neglected the contribution from fields inside the metal. The electric fields can be easily obtained from Eq. (1.2) by using Maxwell's equations: $E_x=\frac{i}{\omega\varepsilon_0\varepsilon_s}\partial_yH_z$ and $E_y=-\frac{i}{\omega\varepsilon_0\varepsilon_s}\partial_xH_z$. Specifically, E_y field can be written as

$$E_y^{x\geq 0}(x,y) = -\frac{Z_0}{k_0\varepsilon_s}\left[q_x \frac{y}{|y|}\left(e^{-iq_x x} + Re^{iq_x x}\right)e^{iq_y|y|} - \int_{-\infty}^{\infty} dk_y \rho(k_y) B(y,k_y) k_x e^{ik_x x} \right]$$
$$E_y^{x\leq 0}(x,y) = -\frac{Z_0}{k_0\varepsilon_s}\int_{-\infty}^{\infty} dk_y \tau(k_y) k_x e^{ik_y y - ik_x x} \quad (1.3),$$

where $Z_0 \equiv \sqrt{\mu_0/\varepsilon_0}$ is the free-space impedance. Now we can readily apply boundary conditions. The continuity of tangential components of magnetic and electric fields (H_z and E_y) at x=0 gives the continuity conditions in real space:

$$\frac{y}{|y|}(1-R)e^{iq_y|y|} + \int_{-\infty}^{\infty} dk_y \rho(k_y) B(y,k_y) = \int_{-\infty}^{\infty} dk_y \tau(k_y) e^{ik_y y} \quad (1.4.1).$$

$$\frac{y}{|y|} q_x (1+R) e^{iq_y|y|} - \int_{-\infty}^{\infty} dk_y \rho(k_y) B(y,k_y) k_x = \int_{-\infty}^{\infty} dk_y \tau(k_y) k_x e^{ik_y y} \quad (1.4.2).$$

We can project the boundary condition Eq. (1.4.1) onto the 2DSP eigenfucntion and the unbounded eigenfunctions of the thin metal region, and Eq. (1.4.2) on to the basis of the free-space region (i.e. plane waves), which yields the following set of integral equations:

$$(1-R)\int_{-\infty}^{\infty} dy e^{2iq_y|y|} = 2\pi \int_{-\infty}^{\infty} dk_y \tau(k_y) A^*(k_y),$$
$$\tau(k_y) = -2\frac{k_y - q_y}{q_y}\rho(k_y) - \frac{1}{\pi i}\int_{-\infty}^{\infty} dk_{y1} \tau(k_{y1}) K(k_{y1}, k_y), \quad (1.5),$$
$$\tau(k_y) = -\frac{2q_y}{k_y + q_y}\rho(k_y) - \frac{q_x}{k_x}(1+R)A^*(k_y) + \frac{2}{i\pi}\int_{-\infty}^{\infty} dk_{y1} \rho(k_{y1}) \frac{q_y}{k_{y1} + q_y} \frac{k_{x1}}{k_x} K(k_{y1}, k_y)$$

where $A(k_y) \equiv \frac{1}{2\pi}\int_{-\infty}^{\infty} dy \frac{y}{|y|} e^{iq_y|y|} e^{-ik_y y}$ is the amplitude of a plane-wave component of Fourier-transformed 2DSP, $K(k_{y1}, k_y) \equiv \frac{k_y}{q_y}\frac{k_{y1}}{k_{y1}^2 - k_y^2}$ is a kernel the second integral, and $k_{xj} \equiv \sqrt{\varepsilon_s k_0^2 - k_{yj}^2}$ with j a positive integer. From the first line of Eq. (1.5), we can see that the reflection coefficient R can be obtained when $\tau(k_y)$ is fixed. The amplitudes of two diffracting wave components, $\tau(k_y)$

and $\rho\left(k_y\right)$, can be obtained by solving the system of two coupled integral equations in the second and third lines of Eq. (1.5). In the following two subsections, we will deal with the integral equation in two different methods.

1-2 Successive approximation method for the integral equation

Note that Eq. (1.5) is a coupled Fredholm integral equation of the second kind. Depending on the kernel type, there could be a known exact solution. However, because the kernel of our case is not in a simple form, we will try the so-called successive approximation method (SAM)[3]. For instance, SAM allows us to approximate $r\left(k_y\right)$ through a recursive scheme such that

$$\tau_n\left(k_y\right) = -2\frac{k_y - q_y}{q_y}\rho\left(k_y\right) - \frac{1}{\pi i}\int_{-\infty}^{\infty} dk_{y1}\tau_{n-1}\left(k_{y1}\right)K\left(k_{y1}, k_y\right)$$

where $\tau_n\left(k_y\right)$ is the *n*-th approximation of $\tau\left(k_y\right)$ and $\lim_{n\to\infty}\tau_n\left(k_y\right)$ saturates to the exact solution independently of the choice an initial trial function $\tau_0\left(k_y\right)$. Let us approximate the second integral in Eq. (1.5) first. The 2nd SAM gives

$$\tau\left(k_y\right) \approx -2\frac{k_y - q_y}{q_y}\rho\left(k_y\right) + \frac{2}{\pi i}\int_{-\infty}^{\infty} dk_{y1}\frac{k_{y1} - q_y}{q_y}\rho\left(k_{y1}\right)K\left(k_{y1}, k_y\right)$$

Then, we can rewrite Eq. (1.5) as

$$\begin{aligned}
&\left(1-R\right)\int_{-\infty}^{\infty} dy e^{2iq_y|y|} = 2\pi\int_{-\infty}^{\infty} dk_y\tau\left(k_y\right)A^*\left(k_y\right),\\
&\rho\left(k_y\right)\frac{2k_y^2 - 4q_y^2}{q_y\left(k_y + q_y\right)} \approx \frac{q_x}{k_x}\left(1+R\right)A^*\left(k_y\right) - \frac{2}{\pi i}\int_{-\infty}^{\infty} dk_{y1}\rho\left(k_{y1}\right)K\left(k_{y1}, k_y\right)\left[\frac{q_y}{k_{y1}+q_y}\frac{k_{x1}}{k_x} - \frac{k_{y1}-q_y}{q_y}\right]\\
&\tau\left(k_y\right) = -\frac{2q_y}{k_y+q_y}\rho\left(k_y\right) - \frac{q_x}{k_x}\left(1+R\right)A^*\left(k_y\right) + \frac{2}{i\pi}\int_{-\infty}^{\infty} dk_{y1}\rho\left(k_{y1}\right)\frac{q_y}{k_{y1}+q_y}\frac{k_{x1}}{k_x}K\left(k_{y1}, k_y\right),
\end{aligned}$$

(1.6).

The second line of Eq. (1.6) is an uncoupled integral equation for $\rho\left(k_y\right)$ that can be rewritten in a simpler form,

$$
\begin{aligned}
& r\left(k_y\right) \approx f\left(k_y\right)+\frac{1}{\pi i} \int_{-\infty}^{\infty} dk_{y1} r\left(k_{y1}\right)\left[\widetilde{K_a}\left(k_{y1}, k_y\right)-\widetilde{K_b}\left(k_{y1}, k_y\right)\right] \\
& \text{with } r\left(k_y\right) \equiv \rho\left(k_y\right) \frac{2k_y^2-4q_y^2}{q_y\left(k_y+q_y\right)}, \quad f\left(k_y\right) \equiv \frac{q_x}{k_x}(1+R) A^*\left(k_y\right), \\
& \widetilde{K_a}\left(k_{y1}, k_y\right) \equiv \frac{k_{y1}^2-q_y^2}{k_{y1}^2-2q_y^2} K\left(k_{y1}, k_y\right), \quad \widetilde{K_b}\left(k_{y1}, k_y\right) \equiv \frac{q_y^2}{k_{y1}^2-2q_y^2} \frac{k_{x1}}{k_x} K\left(k_{y1}, k_y\right)
\end{aligned}
\tag{1.7}
$$

Putting $\rho_n\left(k_y\right)$ into the third line of Eq. (1.6) gives *n*-th approximation of $\tau\left(k_y\right)$ as well as an approximated reflection coefficient, R_n.

To start SAM for Eq. (1.7), let us choose the initial function $r_0\left(k_y\right)=0$. Physically, this corresponds to the single mode approximation of coupled mode theory as it is effectively same with considering that only bounded 2DSP is coupled from the edge reflection. $r_0\left(k_y\right)=0$ gives rise to

$$
\begin{aligned}
& \rho_0\left(k_y\right)=0, \quad \tau_0\left(k_y\right)=(1+R) \frac{q_x}{k_x} A\left(k_y\right), \quad R_0=\frac{1-2 \pi q_y \int_{-\infty}^{\infty} dk_y \frac{q_x}{i k_x}\left|A\left(k_y\right)\right|^2}{1+2 \pi q_y \int_{-\infty}^{\infty} dk_y \frac{q_x}{i k_x}\left|A\left(k_y\right)\right|^2}, \\
& \text{For } q_x >> \sqrt{\varepsilon_s} k_0, \quad R_0 \approx \frac{1-2 / \pi i}{1+2 / \pi i}, \quad \left|R_0\right| \approx 1, \quad \arg\left(R_0\right) \approx 0.361 \pi
\end{aligned}
\tag{1.8}
$$

We note that results in Eq. (1.8) are exactly same with those from earlier works in which single mode approximation is considered[4,5]. A deeper physical meaning of R_0 can be found if we rewrite it in the notion of effective impedance,

$$
R_0=\frac{Z_{0 e f f}-Z_{s p}}{Z_{0 e f f}+Z_{s p}} \tag{1.9}
$$

Here, $Z_{sp} \equiv Z_0 q_x / (\varepsilon_s k_0)$ is the wave impedance of 2DSP, and Z_{0eff} is the initial effective impedance of the evanescent wave of 2DSP in the free-space defined by

$$Z_{0eff}^{-1} \equiv \frac{\int_{-\infty}^{\infty} dk_y Z_{pw}^{-1} \left| A(k_y) \right|^2}{\int_{-\infty}^{\infty} dk_y \left| A(k_y) \right|^2} = \left\langle Z_{pw}^{-1} \right\rangle$$

where $A(k_y)$ and $Z_{pw} \equiv Z_0 k_x / (\varepsilon_s k_0)$ respectively are amplitude and impedance of a plane-wave component of Fourier-transformed 2DSP.

The first approximation for $r(k_y)$ is naturally $r_1(k_y) = f(k_y)$ which gives rise to

$$\begin{aligned}
&\rho_1(k_y) = -(1+R)\frac{q_x}{k_x} A(k_y) \frac{1}{2} \frac{q_y (k_y + q_y)}{k_y^2 - 2q_y^2}, \\
&\tau_1(k_y) = (1+R)\frac{q_x}{k_x} A(k_y) \frac{k_y^2 - q_y^2}{k_y^2 - 2q_y^2} \left(\sqrt{2} + \frac{q_y^2}{k_y^2 - q_y^2} \right), \\
&R_1 = \frac{1 - 2\pi q_y \int_{-\infty}^{\infty} dk_y \left| A(k_y) \right|^2 \frac{q_x}{ik_x} \frac{k_y^2 - q_y^2}{k_y^2 - 2q_y^2} \left(\sqrt{2} + \frac{q_y^2}{k_y^2 - q_y^2} \right)}{1 + 2\pi q_y \int_{-\infty}^{\infty} dk_y \left| A(k_y) \right|^2 \frac{q_x}{ik_x} \frac{k_y^2 - q_y^2}{k_y^2 - 2q_y^2} \left(\sqrt{2} + \frac{q_y^2}{k_y^2 - q_y^2} \right)}, \qquad (1.10). \\
&\text{For } q_x >> \sqrt{\varepsilon_s} k_0, \quad R_1 \approx \frac{1 - \frac{2}{\pi i} \left(\ln(2) \left(1 + \sqrt{2} \right) - 1 \right)}{1 + \frac{2}{\pi i} \left(\ln(2) \left(1 + \sqrt{2} \right) - 1 \right)}, \quad |R_1| \approx 1, \ \arg(R_1) \approx 0.258\pi
\end{aligned}$$

We can see that, for strongly confined 2DSP, the phase of reflection coefficient has been significantly modified from the initial value, whereas its amplitude remains unchanged. It is interesting to see that the limiting value of R_1 for $q_x >> \sqrt{\varepsilon_s} k_0$ is in the same form with R_0 except for the correction term coming from the presence of backward diffracting waves. This allows us to rewrite R_1 as

$$R_1 = \frac{Z_{1eff} - Z_{sp}}{Z_{1eff} + Z_{sp}} \tag{1.11}$$

with Z_{1eff} the corrected effective impedance

$$Z_{1eff}^{-1} \approx Z_{0eff}^{-1}\left(\ln(2)\left(1+\sqrt{2}\right)-1\right) = \left\langle Z_{pw}^{-1}\right\rangle\left(\ln(2)\left(1+\sqrt{2}\right)-1\right).$$

To see the saturating behaviour of the phase, we can go one more step. The second approximation gives $\tau_2(k_y)$, $\rho_2(k_y)$, and R_2 in more complicated forms, but one can obtain the phase shift as

$$\text{For } q_x >> \sqrt{\varepsilon_s}k_0, \quad |R_2| \approx 1, \ \ \arg(R_2) \approx 0.257\pi \tag{1.12}$$

which is slightly changed from R_1, and shows a saturating behaviour. As we discuss in the next subsection, R_1 has only about 3% difference in the phase compared to a more accurate result, arg(R)≈0.250π. We also note that both backward- and forward-diffracting waves are nearly pure-evanescent waves as the amplitude of R is shown to be very close to 1. This means that such anomalous phase shift is related to the phase delay due to the temporal storing of EM energy of 2DSPs in the evanescent waves, which is well known as the Goos-Hänchen phase shift in total in ternal reflection.

1-3. Super-lattice approximation

Another approach to approximate the integral equations in Eqs (1.6) and (1.7) is to quantize the diffracting waves by considering that the system is periodic in y-direction with a sufficiently large periodicity. For an easier treatment, let us assume that the thin metal system is embedded in between two parallel perfect electric conductor (PEC) plates that are located at $y = \pm d$ and infinitely large in x-direction. Note that this configuration makes the system infinitely periodic in y-direction through the image systems. By considering the PEC boundary condition,

$$\partial_y H_z\,|_{y=\pm d}=0,$$

we can rewrite Eq. (1.2) in a quantized form:

$$\begin{aligned}
H_z^{x\geq 0}(x,y) &= \frac{y}{|y|}\left(e^{-iq_x x}-Re^{iq_x x}\right)e^{iq_y|y|}+\frac{y}{|y|}\sum_{n=1}^{\infty}\rho_n\left[e^{i\kappa_{y,n}|y|}+e^{2i\kappa_{y,n}d}e^{-i\kappa_{y,n}|y|}\right]e^{i\kappa_{x,n}x},\\
H_z^{x\leq 0}(x,y) &= \sum_{m=1}^{\infty}\tau_m\sin\left(k_{y,m}y\right)e^{-ik_{x,m}x},\quad \text{with } k_{y,m}\equiv\frac{(2m-1)\pi}{2d},\quad k_{x,m}\equiv\sqrt{\varepsilon_s k_0^2-k_{y,m}^2}
\end{aligned}\tag{1.13}$$

We assumed that d is much larger than the 2DSP wavelength, so that we kept the 2DSP configuration unchanged. A quantized momentum of backward-diffracting wave $\kappa_{y,n}$ is defined by the following eigenvalue equation,

$$2q_y e^{iq_y d+i\kappa_{y,n}d}-q_y e^{2i\kappa_{y,n}d}-\kappa_{y,n}e^{2i\kappa_{y,n}d}=q_y-\kappa_{y,n},$$

that is obtained from PEC boundary condition at $y = \pm d$ and orthogonal condition of backward diffracting waves and 2DSP, and $\kappa_{x,n}\equiv\sqrt{\varepsilon_s k_0^2-\kappa_{y,n}^2}$. Then, we can apply the boundary conditions at x=0. After the same projection procedure used in the previous subsection, we arrive at the following coupled equations:

$$\begin{aligned}
&(1-R)\int_{-d}^{d}dy e^{2iq_y|y|}=\sum_{m=1}^{\infty}\tau_m\widetilde{A}\left(k_{y,m}\right),\quad \text{with } \widetilde{A}\left(k_{y,m}\right)\equiv\int_{-d}^{d}dy\frac{y}{|y|}\sin\left(k_{y,m}y\right)e^{iq_y|y|},\\
&\rho_n=\frac{1+e^{-2i\kappa_{y,n}d}}{2d+\dfrac{\sin\left(2\kappa_{y,n}d\right)}{\kappa_{y,n}}}\sum_{m=1}^{\infty}\tau_m\frac{k_{y,m}}{k_{y,m}^2-\kappa_{y,n}^2},\\
&\tau_m=\frac{1}{d}\frac{q_x}{k_{x,m}}(1+R)A\left(k_{y,m}\right)-\frac{1}{d}\sum_{n=1}^{\infty}\rho_n\frac{\kappa_{x,n}}{k_{x,m}}\left(1+e^{2i\kappa_{y,n}d}\right)\left(\frac{2k_{y,m}}{k_{y,m}^2-\kappa_{y,n}^2}\right)
\end{aligned}\tag{1.14}$$

By truncating the number of quantized modes, Eq. (1.14) can be treated as a matrix algebra. Specifically, the second and third lines of Eq. (1.14) can be rewritten as

$$\begin{aligned}
&\boldsymbol{\rho}=Q\boldsymbol{\tau},\\
&\boldsymbol{\tau}=(1+R)\mathbf{c}-S\boldsymbol{\rho}
\end{aligned}\tag{1.15}$$

with three column vectors $\boldsymbol{\rho}$, $\boldsymbol{\tau}$, and $\mathbf{c}$, and two $N \times N$ matrices Q and S defined as

$$\boldsymbol{\rho}^T \equiv \left[\rho_1, \rho_2, \cdots, \rho_N\right], \quad \boldsymbol{\tau}^T \equiv \left[\tau_1, \tau_2, \cdots, \tau_N\right], \quad \mathbf{c}^T \equiv \left[c_1, c_2, \cdots, c_N\right], \quad c_m \equiv \frac{1}{d}\frac{q_x}{k_{x,m}}\widetilde{A}\left(k_{y,m}\right)$$

$$Q_{mn} = \frac{1+e^{-2i\kappa_{y,m}d}}{2d + \dfrac{\sin\left(2\kappa_{y,m}d\right)}{\kappa_{y,m}}}\frac{k_{y,n}}{k_{y,n}^2 - \kappa_{y,m}^2}, \quad S_{mn} = \frac{1}{d}\frac{\kappa_{x,n}}{k_{x,m}}\left(1+e^{2i\kappa_{y,n}d}\right)\left(\frac{2k_{y,m}}{k_{y,m}^2 - \kappa_{y,n}^2}\right),$$

where N is number of considered diffracting modes. Equation (1.15) gives the solution for $\boldsymbol{\tau}$ as

$$\boldsymbol{\tau} = \left(1+R\right)\left(I+SQ\right)^{-1}\mathbf{c} \tag{1.16},$$

where I is an identity matrix. Combing Eq. (1.16) and the first line of Eq. (1.14), we have the reflection coefficient R as

$$\begin{aligned} R &= \frac{1-\mathbf{a}^T\left(I+SQ\right)^{-1}\mathbf{c}}{1+\mathbf{a}^T\left(I+SQ\right)^{-1}\mathbf{c}}, \\ \text{with } \mathbf{a}^T &\equiv \left[a_1, a_2, \cdots, a_N\right], \quad a_m \equiv \frac{\widetilde{A}\left(k_{y,m}\right)}{\int_{-d}^{d} dy e^{2iq_y|y|}} \end{aligned} \tag{1.17}.$$

For $q_x \gg \sqrt{\varepsilon_s}k_0$, one can find that Eq. (1.17) gives the phase shift as

$$\arg\left(R\right) \approx 0.250\pi \tag{1.18}.$$

Shown in Fig. S2 is a comparison of even-odd peak oscillations calculated from two methods we discussed so far. It is worth noting that, compared to results from the super-lattice method, the second approximation of SAM already gives reasonably accurate field profiles, and that the reflection coefficient from the first approximation of SAM shown in Eq. (1.10) has only about 3% difference in phase.

1-4. Surface polaritons in 2D hyperbolic media

Hexagonal Boron Nitride (hBN) is a prime example of a uniaxial material supporting hyperbolic phonon polariton (PhP) modes. In such hyperbolic media, the allowed SP modes can be different from those in simple metals slabs. Specifically, for a free-standing hyperbolic material, the dispersion relation of surface polariton is given by

$$\tan\left(\frac{h}{2}\sqrt{\varepsilon_{in}k_0^2-\frac{\varepsilon_{in}}{\varepsilon_{out}}q_x^2}\right)\varepsilon_{in}\sqrt{k_0^2-q_x^2}+i\sqrt{\varepsilon_{in}k_0^2-\frac{\varepsilon_{in}}{\varepsilon_{out}}q_x^2}=0 \quad (odd),$$

$$\cot\left(\frac{h}{2}\sqrt{\varepsilon_{in}k_0^2-\frac{\varepsilon_{in}}{\varepsilon_{out}}q_x^2}\right)\varepsilon_{in}\sqrt{k_0^2-q_x^2}+i\sqrt{\varepsilon_{in}k_0^2-\frac{\varepsilon_{in}}{\varepsilon_{out}}q_x^2}=0 \quad (even),$$

where ε_{in} and ε_{out} are in-plane and out-of-plane permittivities of the hyperbolic material, respectively. In principle, if we consider PhPs in hBN, we have to take into account higher order of both in-plane (odd) and out-of-plane (even) PhP modes to have accurate description of the propagation of PhPs, especially when the thickness of hBN is comparable to the PhP wavelength. However, in the 2D-limit where the thickness of hBN goes to deep sub-polariton-wavelength regime, we note that only the fundamental in-plane mode can be mainly observable in experimental studies. For $\varepsilon_{in}<0$, $\varepsilon_{out}>0$, one can find from the above equation that the momentum of first-excited in-plane modes in the 2D-limit can be approximately written as

$$q_{x,in}^{1st} \approx q_{x,in}^{fund} + \sqrt{-\frac{\varepsilon_{out}}{\varepsilon_{in}}}\frac{2\pi}{h}.$$

where $q_{x,in}^{fund}$ is the momentum of fundamental in-plane mode. Excitation of all higher modes will be strongly suppressed due to extraordinarily large polariton momenta yielding extremely low photon-phonon coupling efficiency, and this trend becomes stronger as the thickness gets thinner. Also, one can find that the fundamental out-of-plane PhP mode is mostly confined inside the hBN

layer. Therefore, compared to that of the in-plane case, the PhP-tip coupling of our-of-plane case is very weak[6]. The propagation property of fundamental in-plane PhP mode is exactly same with that of two-dimensional surface plasmons such as graphene plasmons, exhibiting anti-symmetric configuration of the normal-component of electric field in the proximity of material's surfaces. This nature of PhP is discussed in detail in the previous work[6], and is the reason that our main theoretical predictions, anomalous phase shift and even-odd peak oscillations in the edge-reflection, are also observed in thin hBN flakes in earlier experimental studies[6,7].

2. Phase extraction from experimental measurements

To measure the reflection phase shift experimentally, the tip-scattered near field signal E_{N} is homodyne interfered with the reference E_{ref} of a Michelson interferometer with beam-splitter. To suppress the signal from the interference between the near field and the uncontrollable background E_{bg} (mainly from the tip and substrate), we used a strong reference beam[8]. The measured near field signal at distance x away from the edge is due to the interference between the tip launched polariton field and edge reflected polariton field.

$$I_{measured} \propto E_{ref} E_N^{inc} \left|1+\left|R\right|\cos(2q_x x+\phi_R)\right| \tag{2.1}$$

Where E_N^{inc} is the amplitude of tip launched wave, R is the reflection coefficient and ϕ_R is the reflection phase. The peak positions of the measured signal obtained in near field image will be determined in terms of $q_x x$ and ϕ_R. This means that all required parameters to obtain the phase shift ϕ_R are the wavelength of 2DSPs, and the distance between the edge and a peak. The position of the edge of the graphene is identified from the topography image which is simultaneously

obtained during the scanning. The wavelength of 2DSPs can be fixed by measuring the distance between two neighboring peaks. Because our theory predicts that the position of the first peak can be strongly disturbed by the back-scattering diffraction of 2DSPs, second and third peaks are used to determine the wavelength, and the third peak is used to measure the distance from the edge. Then, the phase shift can be calculated from the following equation:

$$\phi_R = 2\pi \times 3 - \frac{4\pi}{\lambda_{sp}}\left(x_3 - x_e\right) = 2\pi\left(3 - \frac{x_3 - x_e}{x_3 - x_2}\right) \quad (2.2),$$

where x_e, x_2, and x_3 respectively are positions of the edge, second peak, and third peak. Fig. S3(a) shows an exemplary near-field image of graphene at gate voltage -100V with incident light 10.6 μm. Fig. S3(b) is a cross-cut profile of the inference pattern taken along the line in Fig. S3(a). Positions for the second/third peaks, and the edge are indicated in the image.

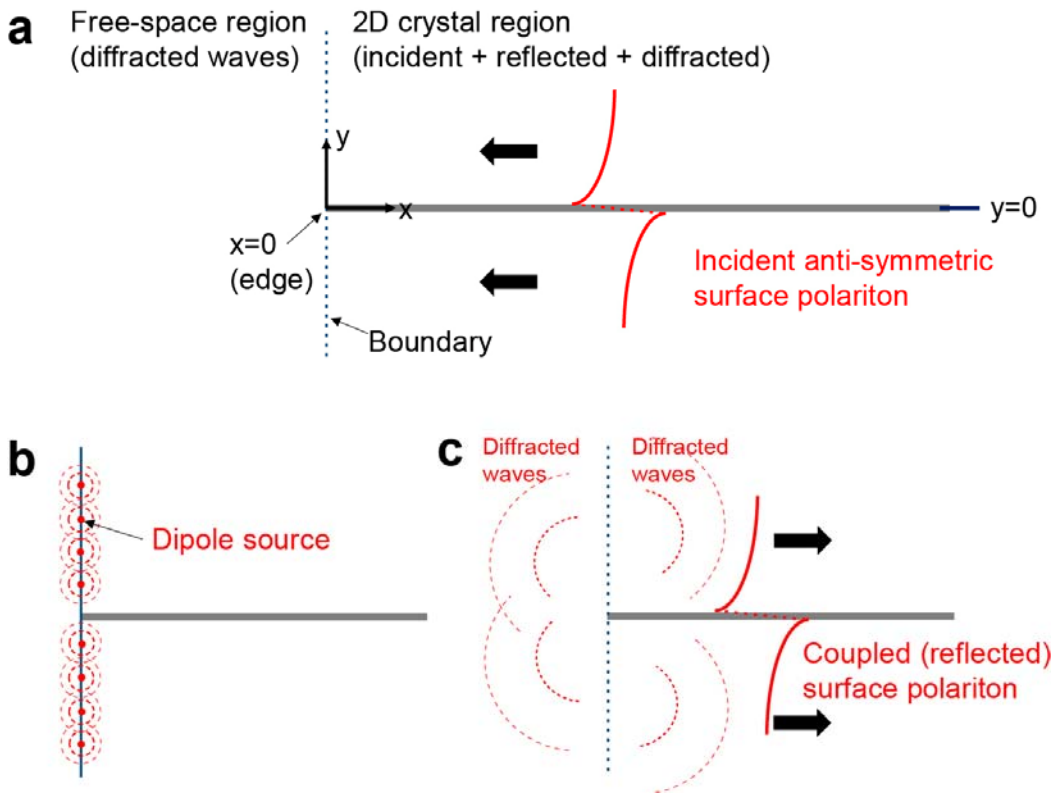

Figure S1. Macroscopic procedure of edge-reflection of 2DSPs. **a**. A schematic of the system. 2DSPs is incident from right. **b**. Dipole sources coupled from the incident 2DSPs. Diffracting waves are in the form of outgoing waves generated from the dipole sources. **c**. Coupling of 2DSPs from the diffracting waves that results in the edge-reflection of 2DSPs.

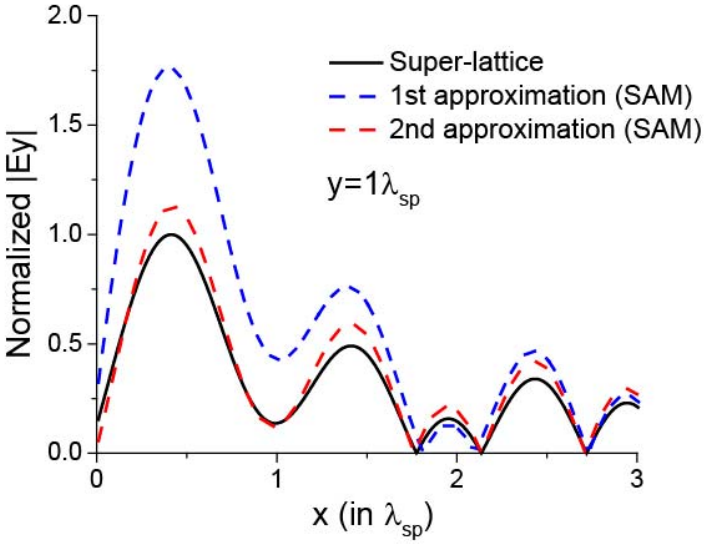

Figure S2. A comparison between SAM and super-lattice approximation. In order to see the accuracy of backward diffracting waves calculated by SAM, even-odd peak oscillations at $y = \lambda_{sp}$ are considered. For the super-lattice approximation, we truncated the mode number as $N = 7{,}500$ and set $d = 50\lambda_{sp}$. In every calculation, we set $q_x = 50k_0$ and ε_s=1.

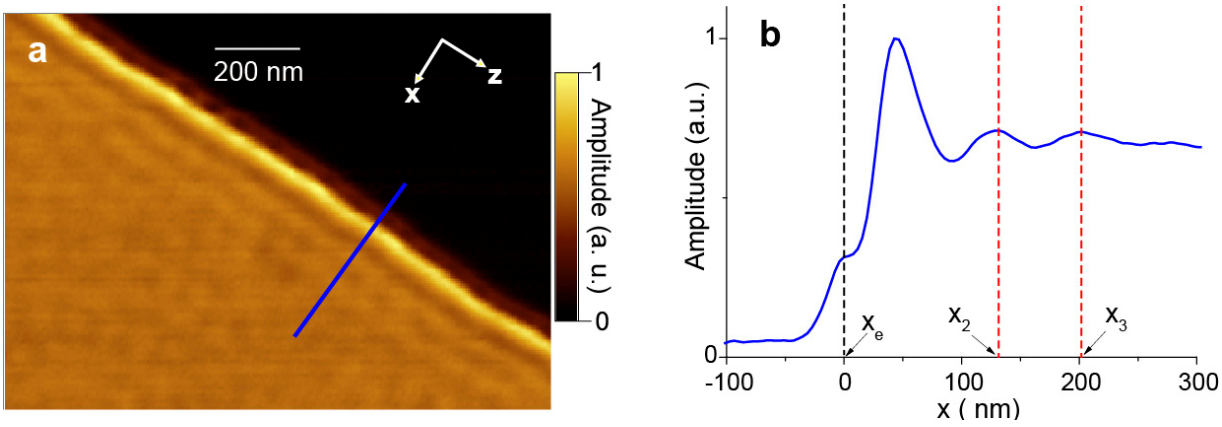

Figure S3. Phase extraction from experimental results. a, Near-field image of graphene at gate voltage -100 V with incident light 10.6 μm. **b**, Cross-cut profile of the inference pattern taken along the line in **a**.

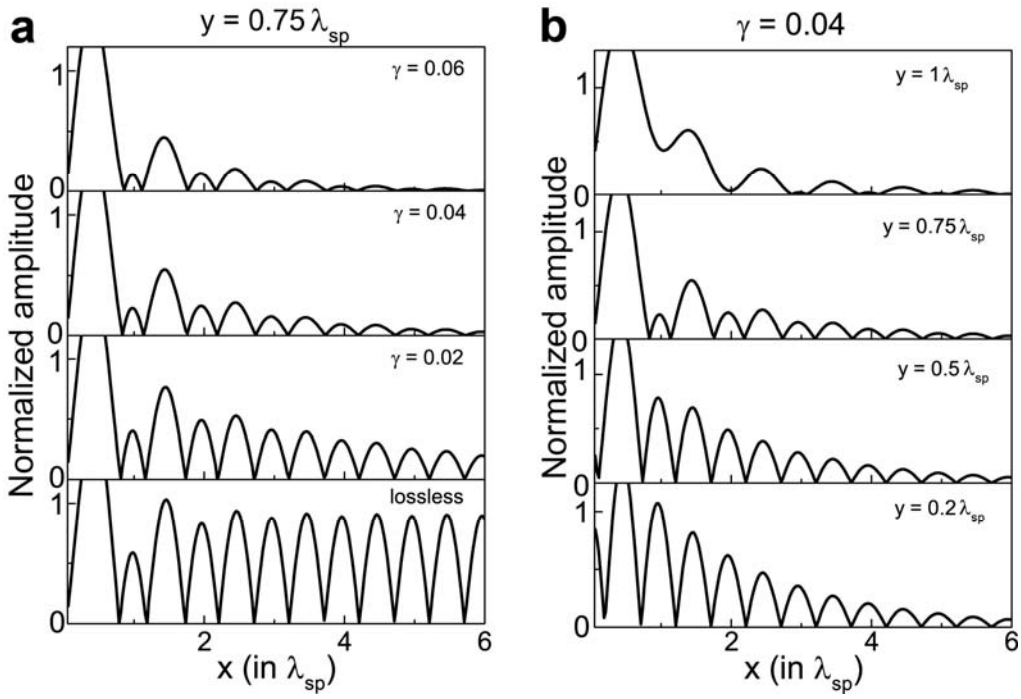

Figure S4. Even-odd peak oscillations with material loss. a, The peak oscillations with different damping rate γ at y = 0.75 λ_{sp}. For a given damping rate, the decay of 2DSP can be calculated by $\exp(2q_{xr}\gamma x)$ where q_{xr} is the real part of q_x. One can find that γ is equivalent to q_{xi}/q_{xr} of which q_{xi} the imaginary part of q_x. We can clearly see that the even-odd peak oscillations become more pronounced with a higher material loss. **b**, Height-dependent peak oscillation with γ=0.04.

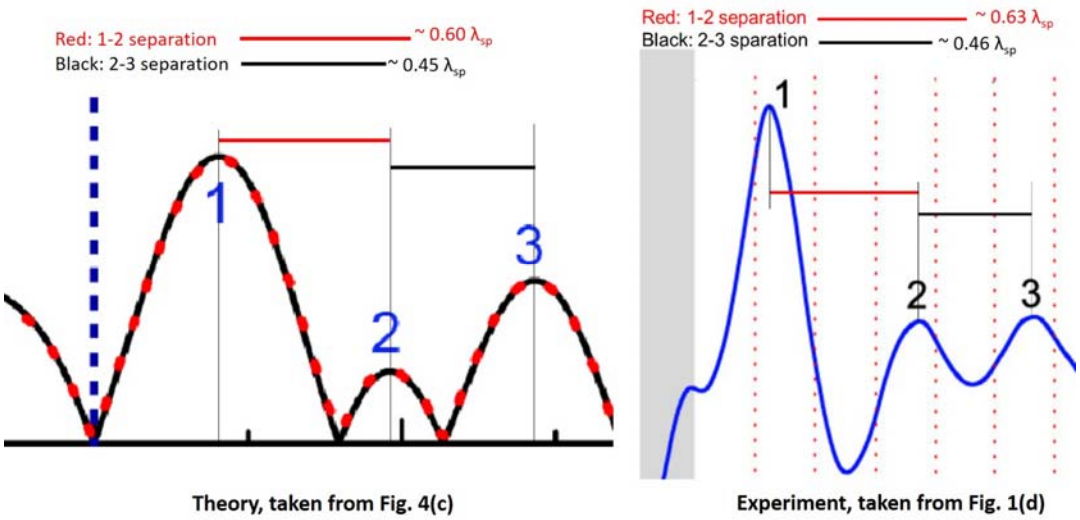

Figure S5. Separations between the 1st-2nd peaks and 2nd-3rd peaks. In both analytic and experimental results, it is clearly shown that 1-2 separation is larger than 2-3 separation. Note that the origin of this different peak separation is the interference of 2DSPs with back-diffracting evanescent waves.

References

(1) Alù, Andrea, Engheta, N. *J. Opt. Soc. Am. B* **2006**, *23*, 571–583.

(2) Jackson, J. D. *Classical Electrodynamics 3rd Edition*; John Wiley & Sons, INC., 1999.

(3) Zemyan, S. M. *The Classical Theory of Integral Equations*; Birkhäuser: Boston, 2012.

(4) Nikitin, A. Y.; Low, T.; Martin-Moreno, L. *Phys. Rev. B* **2014**, *90*, 041407(R).

(5) Du, L.; Tang, D.; Yuan, X. *Opt. Express* **2014**, *22*, 749–758.

(6) Shi, Z.; Bechtel, H. A.; Berweger, S.; Sun, Y.; Zeng, B.; Jin, C.; Chang, H.; Martin, M. C.; Raschke, M. B.; Wang, F. *ACS Photonics* **2015**, *2*, 790–796.

(7) Dai, S.; Fei, Z.; Ma, Q.; Rodin, A. S.; Wagner, M.; McLeod, A. S.; Liu, M. K.; Gannett, W.; Regan, W.; Watanabe, K.; Taniguchi, T.; Thiemens, M.; Dominguez, G.; Neto, A. H. C.; Zettl, A.; Keilmann, F.; Jarillo-Herrero, P.; Fogler, M. M.; Basov, D. N. *Science* **2014**, *343*, 1125–1129.

(8) Gerber, J. A.; Berweger, S.; O'Callahan, B. T.; Raschke, M. B. *Phys. Rev. Lett.* **2014**, *113*, 55502.